

State of Charge Estimation for Lithium-Ion Battery Models Based on a Thermoelectric Coupling Model

Huanhuan Li^{1,3}, Xiaoyu Wang¹, Ashwani Saini¹, Yuqiang Zhu¹, Ya-Ping Wang^{2,3,*}

¹ Automotive Engineering Research Institute, Jiangsu University, 301 Xuefu Road, Zhenjiang 212013, P. R. China

² School of Materials Science & Engineering, Jiangsu University, Zhenjiang 212013, P. R. China

³ Key Laboratory of Advanced Energy Materials Chemistry (Ministry of Education), College of Chemistry, Nankai University, 94 Weijing road, Tianjin, 300071, PR China

*E-mail: wangyaping@ujs.edu.cn

Received: 2 December 2019 / *Accepted:* 8 February 2020 / *Published:* 10 April 2020

Conventional equivalent circuit models of lithium-ion batteries (LIBs) ignore the influence of temperature changes caused by heat generated inside the battery; unfortunately, the above leads to mismatched model parameters, which decreases the precision of the model. In this paper, a thermoelectric battery model based on thermoelectric coupling is proposed by coupling an equivalent circuit model with a thermal model, which considers the temperature increase in the battery. Performance tests for the hybrid pulse power characteristic (HPPC), charge-discharge capacity-voltage curve, time-temperature curve and direct current (DC) internal resistance were performed to calibrate 30 Ah ternary prismatic LIBs; furthermore, the model parameters were identified by a least squares method. The accuracy and effectiveness of the model were then validated by steady-state experiments and dynamic tests. In the steady state experiment, the maximum voltage error was 24.36 mV, and the maximum temperature simulation error was 0.93 °C at 1C, whereas the absolute voltage error was under 20 mV and the error of a high current pulse reached 60 mV in a dynamic test under the New European Driving Cycle (NEDC) condition. The above results confirm that the simulation can consistently and properly model the experimental results, which illustrates that the developed model has high accuracy and can reflect the characteristics of LIBs during a charge/discharge process in real time. Finally, an SOC estimation method for an LIB is developed by using an extended Kalman filter algorithm and is verified by experiments under the NEDC condition. The results show that the model has a high estimation accuracy, and the SOC error, maximum error and average error values are approximately 3%, 2.96% and 0.81%, respectively; additionally, an initial value dependence or a cumulative error in an ampere-time integration method is not generated, which demonstrates that the algorithm has a strong self-correcting ability with initial SOC errors and strong convergence.

Keywords: Lithium-ion battery; Thermoelectric coupling model; Equivalent circuit; Parameter identification; SOC Estimation

1. INTRODUCTION

Hybrid, plug-in hybrid electric and electric vehicles have been widely developed due to the energy crisis and the outbreak of global warming[1-2]. Batteries are the power source and the key point in the development of electric vehicles. Recently, compared with other batteries, lithium-ion batteries (LIBs) have been widely used not only because of their high density, high power density, long cycling life and environmental friendliness [1] but also because of their low self-discharge rate and lack of a memory effect [2]. However, LIBs have problems with reliability and safety, especially under extreme conditions, which may cause serious safety problems such as spontaneous combustion and explosion. In a battery management system (BMS), an accurate estimation of the battery state can prolong the service life of a power battery pack, improve the cruising range and prevent the safety problems caused by overcharge and overdischarge; however, the estimation of the battery state depends on establishing an accurate battery model[3].

Mainstream battery models mainly include electrochemical models and electrical models. Compared with electrical models, electrochemical models are established based on their electrochemical reaction mechanism, which can essentially reflect the relationship between the external characteristics and internal parameters, which helps provide highly accurate SOC estimations. Therefore, electrochemical models of LIBs have been widely studied in recent years. In 1989, Evans and Ehite et al. used a two-dimensional thermal model to study the internal temperature field of a cylindrical LIB. For the first time, the characteristics of the anisotropy of various materials inside the battery were considered [4-5]. Lee et al. established a thermo-electro-electrochemical coupling model based on a continuous model of potential and studied the temperature field and current phase of the current [6]. Doyle et al. proposed a P2D (Pseudo 2 Dimensions) model for LIBs. The model describes the charging and discharging process of LIBs based on Li^+ deintercalation and concentration changes [7-9]. In our previous work, we have reported some research on electrochemical models of LIBs, such as a simplified average electrode electrochemical model for LIBs, in which the order of solid and electrolyte phase diffusion equations was reduced by a polynomial approximation and a trivariate method; notably, the above showed high accuracy and high robustness [10]. In addition, an electrochemical model of LIBs that considers the effect of a double electric layer potential on the overpotential and an extended single particle (ESP) electrochemical model that considers the effect of an electrolyte phase potential on the terminal voltage have been designed [11-12]. Both works exhibit highly accurate and reliable SOC estimations.

However, there are many partial differential and state equations in electrochemical models, which are hard to analyze and generate dozens of undetermined parameters. Thus, these tasks are computationally intensive, and the parameters obtained are complicated and unsuitable for engineering applications.

Compared with the electrochemical model, an equivalent circuit model abstracts the electrochemical characteristics of a battery and expresses them by electrical components; thus, equivalent circuit models are easier to implement. Because of their simple structure and small amount of calculation, it is currently the first choice for real-time control systems and practical engineering applications.

Kirill et al. [13] established a thermal-electric coupled model for LIBs in hybrid electric vehicles, which integrated a three-dimensional thermal model with an equivalent circuit model and determined the thermophysical parameters according to empirical values. Yoon et al.[14] studied the change rule of discharge resistance over time and its power characteristics according to changes in the charge discharge state and storage temperature. However, the influence of battery temperature on internal parameters has not been considered in the above studies, and some of them only considered the influence of ambient temperature on the internal parameters of the battery.

Therefore, to improve the accuracy of a BMS, the impact of temperature on an LIB model has more practical value and needs to be considered. Since a battery is a complex nonlinear system, a simple Thevenin model has difficulty accurately describing the behavior of batteries, whereas a multistage RC model is too complicated to recognize the parameters, and its amount of calculation is too large for practical application toward a vehicle system. Therefore, this paper uses a second-order RC equivalent circuit model based on a Thevenin model [3]; the above can show the two polarization processes, more accurately reflect the dynamic characteristics of the battery, and at the same time, keep it from getting too complicated, thus reducing the amount of computation [15].

Herein, a thermoelectric model is established by coupling the improved second-order Thevenin model with an equivalent thermal model of the battery. HPPC, charge-discharge, time-temperature and DC internal resistance tests are performed to calibrate the electrochemical performance of 30 Ah ternary prismatic LIBs, and the model parameters are identified by a least squares method. The accuracy of the model is then validated by steady-state experiments and dynamic tests. Furthermore, an SOC estimation method of the LIB is developed by using an extended Kalman filter and is verified by New European Driving Cycle (NEDC) condition experiments. The research route of this paper is shown in Figure 1.

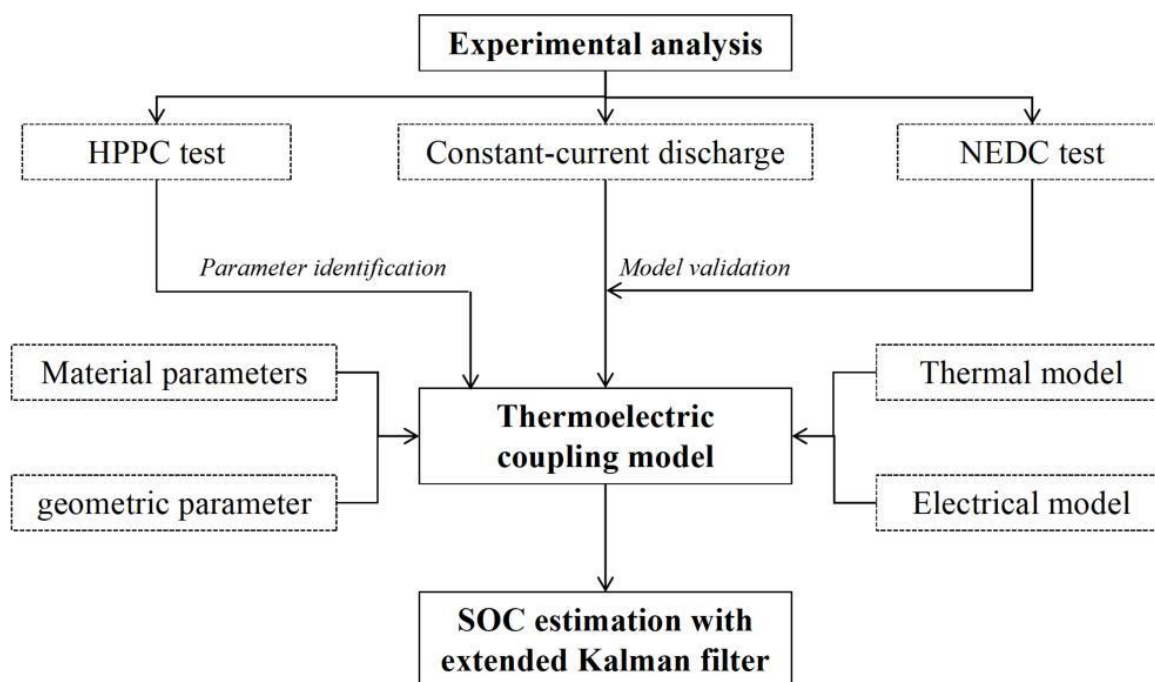


Figure 1. Technical route.

2. MODEL ESTABLISHMENT

2.1 Establishment of the second-order equivalent circuit model

Because it is difficult to accurately describe the behavior of a battery with a Thevenin model and a multistage RC model is too complicated to recognize the parameters and requires considerable calculation, this work adopts a second-order RC equivalent circuit model based on an improved Thevenin model. As shown in Figure 2, the second-order RC equivalent circuit model is based on the Thevenin model, which subdivides the effect caused by the polarization of internal resistance into electrochemical polarization and concentration difference polarization.

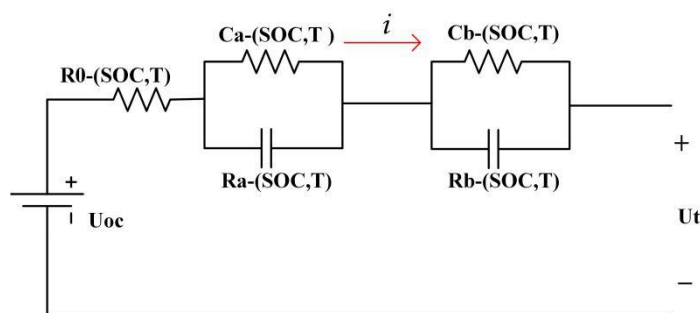


Figure 2. Thevenin model.

As shown in Figure 2, U_{oc} represents the open circuit voltage (OCV), R_0 is the ohmic internal resistance, C_a is the capacitance caused by the electrochemical polarization, R_a is the resistance caused by the electrochemical polarization, C_b is the capacitance caused by the polarization difference, R_b is the resistance caused by the polarization difference, and U_t represents the terminal voltage of the battery. When the battery is discharged, it can be expressed by the following three equations:

$$\begin{cases} \dot{u}_a = \frac{i}{C_a} - \frac{u_a}{R_a C_a} \\ \dot{u}_b = \frac{i}{C_b} - \frac{u_b}{R_b C_b} \\ u_t = u_{oc} - u_a - u_b - iR_0 \end{cases} \quad (1)$$

2.2 Establishment of the thermal model

The thermal model of the battery is mainly used to calculate the temperature change of the battery during the discharge process. According to the principle of energy conservation, the thermal model describes the relationship between the generation, transmission and dissipation of battery heat. The equivalent thermal model of the electrical model is mainly used to calculate the temperature rise of the battery in practical applications [16]. In this paper, the equivalent thermal model is based on the equivalent circuit model, and the internal reaction of the battery is simplified. Compared with the

electrochemical model, the accuracy of the thermal model is slightly insufficient, but it is more suitable for practical engineering [17].

In the thermal model, the battery temperature T_c is determined by the following equation:

$$T_c = T_0 + \frac{1}{c_c m_c} \int P_w dt \quad (2)$$

where T_c is the real-time temperature; T_0 is the initial temperature of the battery, which is taken as the ambient temperature; C_c is the specific heat capacity of the battery, which is 856 J/kg·K according to the manufacturer; m_c represents the weight of the battery, which is 1.05 kg; and P_w is the power of the battery that absorbs heat during discharge. In this paper, the heat generated by the battery mainly includes the ohmic heat, polarization heat and heat exchange with the environment during the discharge process. Because the temperature is usually higher than the environmental temperature, the heat exchange with the environment is set as the heat dissipation under natural conditions for the battery.

Thus, P_w can be expressed as:

$$\begin{cases} P_w = P_0 + P_a + P_b - P_{loss} \\ P_0 = i^2 R_0 \\ P_a = i^2 R_a \\ P_b = i^2 R_b \\ P_{loss} = hS(T_c - T_0) \end{cases} \quad (3)$$

where P_0 is the thermal power of ohmic internal resistance, P_a is the thermal power of electrochemical polarization resistance, P_b is the heat power of internal resistance from the concentration difference polarization, P_{loss} is the heat dissipation power of the battery, h is the heat convection coefficient with a value of 10 W/(m²×K) according to ref. [16], and S is the surface area of the cell with a value of 0.36635 m².

2.3 Coupling of thermoelectric models

According to equations 1 and 2, the open circuit voltage, ohmic internal resistance, polarization capacitance, and polarization internal resistance in the electrical model are affected by the SOC and temperature of the battery, but their relationship is nonlinear. In this work, the parameters of the battery model under different SOC values and temperatures are determined by the Simulink 2D look-up table method.

A thermoelectric coupling battery model is built on Simulink according to equations 1-3. The outer frame of the model is shown in Figure 3. The SOC calculation module uses a real-time integration method to calculate the SOC of the battery in real time. The RC-thermal module is a thermoelectric coupling module, as shown in Figure 3. The input is the ambient temperature, real-time SOC and current, and the output is the terminal voltage and real-time temperature of the battery.

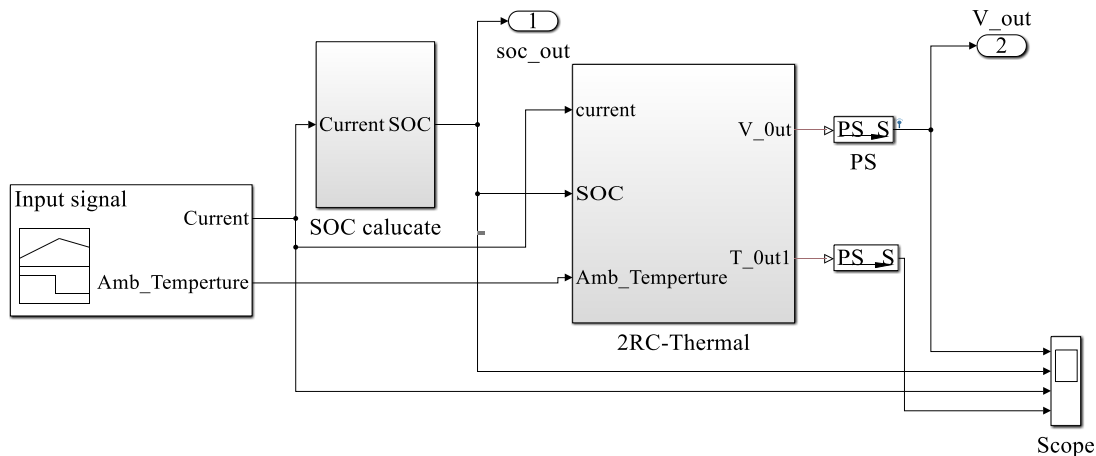


Figure 3. Framework diagram of the thermoelectric coupling model.

The internal structure of the RC-thermal module in the thermoelectric coupling model is shown in Figure 4. The current flows through two RC currents and the ohmic internal resistance. Correspondingly, the total heating power of the two RC currents and the ohmic internal resistance can be calculated according to the heating power resistance. The heating power is fed back to the thermal model, and the calorific value can be obtained by integrating the time. Then, according to thermal model equations 2 and 3, the real-time temperature of the battery current can be calculated, and then the temperature is fed back to the second-order equivalent circuit model; from there, the battery parameters can be obtained by a two-dimensional look-up table method to obtain the corresponding parameters. In turn, the estimation accuracy of the model is optimized.

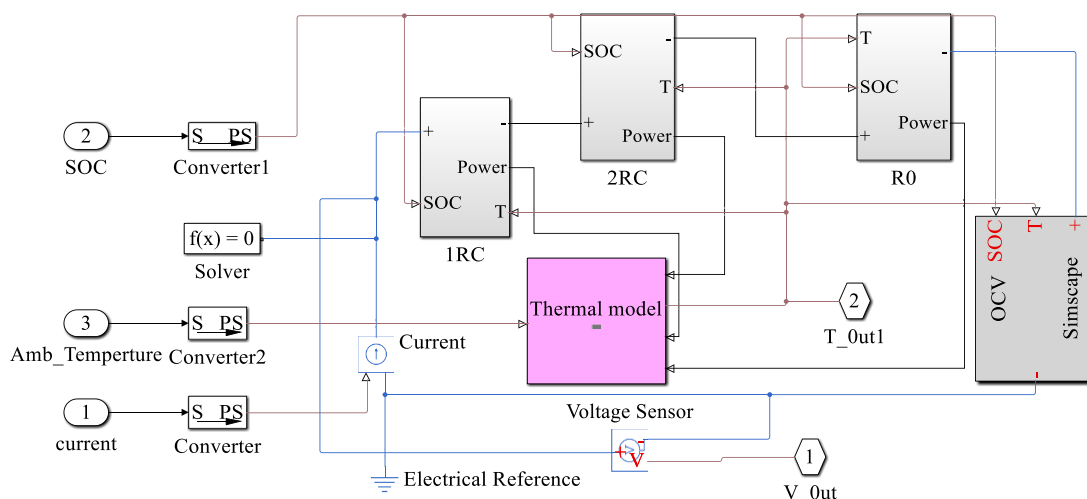


Figure 4. Internal structure of the RC-thermal module of the thermoelectric coupling model.

2.4 Model parameter identification

The parameters need to be identified after the model is built. According to equations 1-3, some parameters in the second-order equivalent circuit model can be measured experimentally, such as the

open circuit voltage U_{oc} and ohmic internal resistance R_0 , whereas some parameters cannot be measured directly and need to be identified in experiments, such as the electrochemical polarization capacitor C_a .

In this work, we selected 30 Ah prismatic ternary LIBs (produced by Jiangsu Chunlan Clean Energy Research Institute Co., LTD) with an operating voltage of 4.2-2.8 V as the research object. The battery test was carried out by using a BTS-5V/10A battery detection system. The surface temperature of the battery was collected by a thermocouple sensor. An MSK-TE906 thermal chamber was used to set the ambient temperature and humidity conditions. The HPPC experimental steps were as follows [18]:

(1) Put the battery in the thermal chamber at a temperature of 25 °C and let it stand for 3 hours. First, the battery was charged to a cut-off voltage of 4.2 V with a constant current (1C) and then the test was changed to a constant voltage (4.2 V), while charging to a cut-off current of 1.5 A (0.05C); afterward, the battery was left standing for 1 hour. The voltage sampling frequency was 1 s in the above process.

(2) The temperature of the thermal chamber was adjusted to 15 °C, and the battery was kept at 15 °C for 2 hours. Then, the battery was discharged at 1C for 10 s with a voltage sampling frequency of 0.1 s. Next, after the battery was left standing for 40 s, it was charged at 0.75 °C for 10 s.

(3) The battery was kept standing for 1 hour with a voltage sampling frequency of 1 s. Then, the battery was discharged at a rate of 1C for 340 s (approximately 10% SOC). Finally, the battery was left standing for 1 hour with a voltage sampling frequency of 1 s.

(4) Steps (3) to (6) were repeated 10 times until the SOC reached 0%.

(5) Steps (1) to (6) were repeated and the temperature of step (2) was adjusted to 20 °C, 25 °C, 30 °C, 35 °C and 40 °C to obtain data for a full temperature gradient.

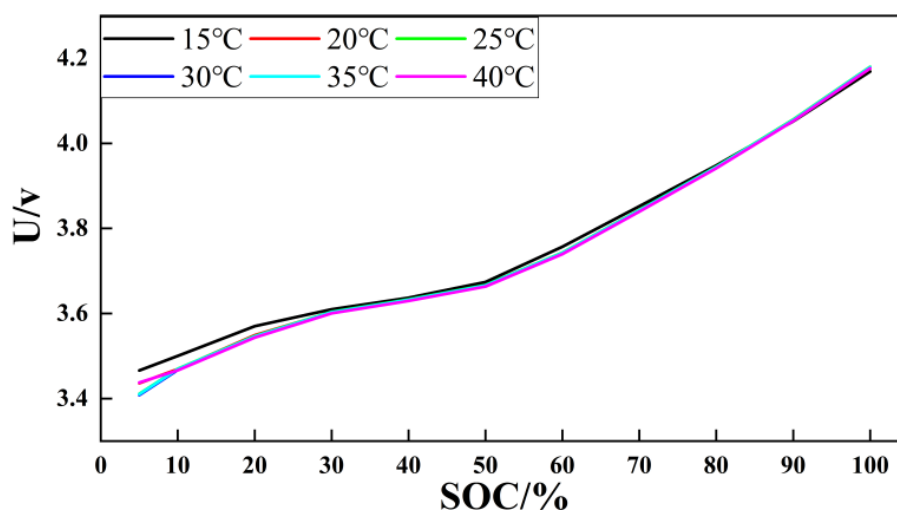


Figure 5. Measured OCV-SOC curves at different temperatures.

The open circuit voltages U_{oc} at different SOC levels can be obtained by the above experiments. Figure 5 shows the OCV-SOC curves at different temperatures. The voltage change is relatively stable when the SOC is in the range of 20%-60%, and the voltage changes faster when the SOC is less than

20% or greater than 60% because the polarization reaction is more serious when the battery is at a low or high SOC.

Since OCV is less sensitive to temperature, the curve fitting of OCV-SOC is only fitted at 25 °C by the curve fitting module of MATLAB and represents the full temperature gradient of OCV-SOC in this work. The fitting curve equation of OCV-SOC is obtained as follows:

$$U_{oc} = 6.234e-10*soc^5 + -2.055e-07*soc^4 + 2.543e-05*soc^3 + -0.001379*soc^2 + 0.03635*soc + 3.213 \tag{4}$$

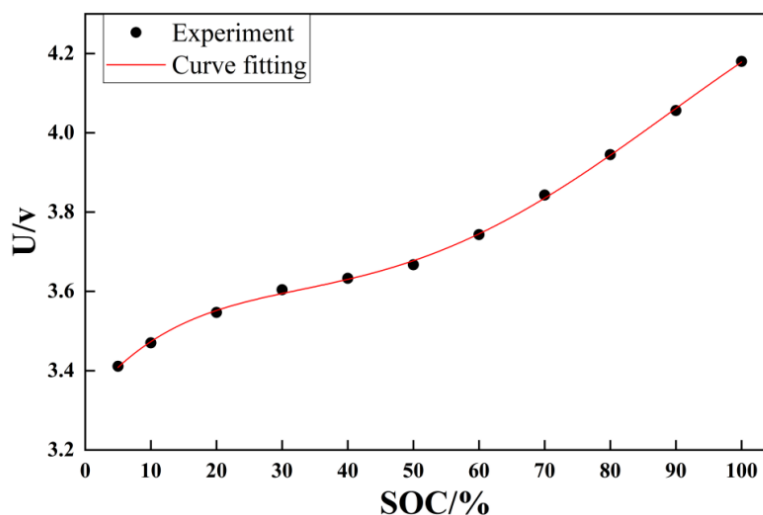


Figure 6. Fitted OCV-SOC curve at room temperature (25 °C).

Figure 7 shows the pulse discharge curve. When the battery is discharged, it can be divided into four stages. The first stage is the t_0-t_1 period, which is the voltage drop caused by the ohmic resistance. The second stage is the t_1-t_2 period, which is the electrochemical polarization, concentration polarization and voltage drop during the battery discharge process. The third stage is the t_2-t_3 period, at which time the voltage rises due to the disappearance of the discharge current. The fourth stage is the t_3-t_4 period, at which time the polarization effect disappears, and the voltage between the electrode oxidation and the reduction reaction reaches equilibrium. At the moment when the current is loaded, the terminal voltage of the battery changes considerably. At this time, the battery has not produced electrochemical polarization or concentration difference polarization, but the ohmic internal resistance polarization is transient, so it is believed that the transient voltage drop at this time is caused by the ohmic internal resistance R_0 [19]. Therefore, the above can be described with the following equation:

$$R = \frac{\Delta U}{I} \tag{5}$$

From Figure 7 and according to equation 5, equation 6 can be calculated as follows:

$$R_0 = \frac{U_0 - U_1}{I_1} \tag{6}$$

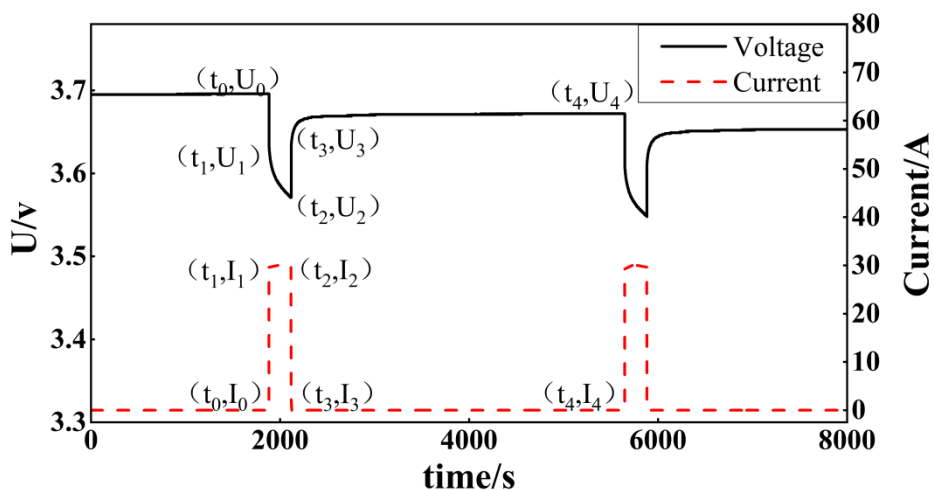


Figure 7. Terminal voltage profiles of the HPPC discharging current.

Furthermore, a three-dimensional surface map can be obtained to show the relationship between the ohmic internal resistance, OCV and temperature by using an interpolation method. As shown in Figure 8, the x -axis represents temperature, the y -axis identifies SOC, and the z -axis represents ohmic internal resistance. It can be seen that when the temperature of the battery is low, the SOC decreases, and the ohmic internal resistance increases; whereas, when the temperature is high, the SOC increases, and the ohmic internal resistance of the battery decreases. These phenomena are due to an increase in the viscosity of the electrolyte, which leads to a decrease in conductivity at a low temperature. Thus, the side effects of the battery are more severe under the condition of a low SOC, which leads to an increase in the internal resistance of the battery under low temperature and SOC conditions.

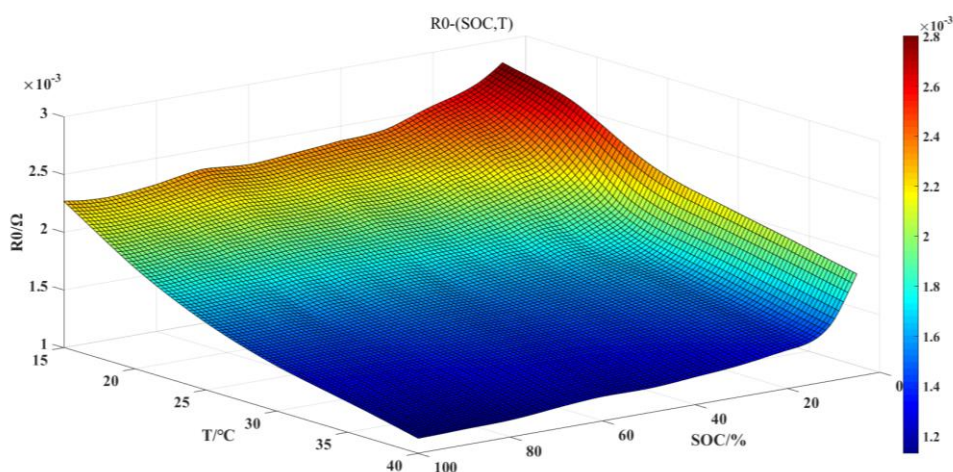


Figure 8. Fitting surfaces of R_0 .

The second stage in the discharge process is part of the voltage drops in Figure 7. At this time, because of the charging of the capacitor, the voltage curve approximates an exponential function drop.

Manipulating with parts of equation 1 provides the following:

$$U_0 = U_{oc} - iR_1 \left(1 - \exp\left(-\frac{t}{\tau_1}\right)\right) - iR_2 \times \left(1 - \exp\left(-\frac{t}{\tau_2}\right)\right) - iR_0 \quad (7)$$

Stage 2 can be properly described according to equation 7, and the remaining parameters, electrochemical polarization capacitance C_a , electrochemical polarization internal resistance R_a , concentration difference polarization capacitance C_b , and concentration difference polarization resistance R_b , can be identified.

3. RESULTS AND DISCUSSION

3.1 Model validation

To verify the accuracy of the thermoelectric coupling model, charge/discharge tests at 1C and NEDC tests were performed.

3.1.1 Constant discharge of electricity at 1C

Figure 9 (a) shows the experimental and simulation terminal voltage curves of the constant discharge test at 1C and 25 °C. The black line is the experimental terminal voltage curve, while the red line is the simulation result. Figure 9 (b) is the voltage error curve of the experimental and simulation results. The simulated voltage of the model is consistent with the actual voltage data in the range of 100%~10% SOC, and the absolute voltage error is less than 25 mV, indicating that the model has high precision. The source of error is mainly divided into two aspects: one is a measurement error in the experimental instrument, and the other is the deviation between the second-order model and the battery characteristics.

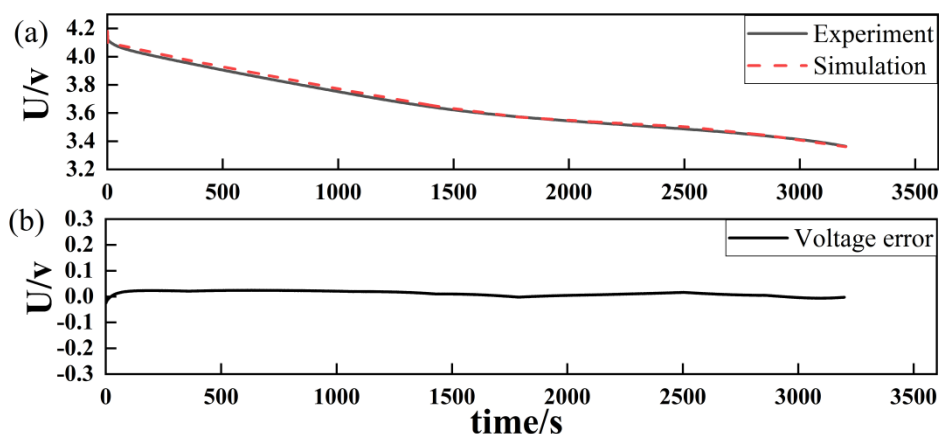


Figure 9. Comparison between the experimental data and simulation results of the test (a) and the absolute voltage error between them (b) at a discharge of 1C.

Figure 10 (a) is the temperature curve of the experiment and simulation at 1C. The black line is the experimental curve, and the red line is the simulation result. The two curves are basically

consistent. Figure 10 (b) is the temperature error curve of the experimental and simulated results. The temperature of the battery rises by 7.4 °C when the SOC is discharged from 100% to 10% at 25 °C with a rate of 1C, which shows that it is more important to consider the temperature of the battery than the influence of the ambient temperature on the battery. At the same time, the simulation results of the established thermal model are also consistent with the actual experimental data. The maximum absolute temperature error is 0.93 °C (Figure 10 (b)). Since the model in this work is based on a simplified thermal model of the electrical model, there is certainly a sacrifice in accuracy. However, this margin of error is acceptable to meet the needs of engineering applications.

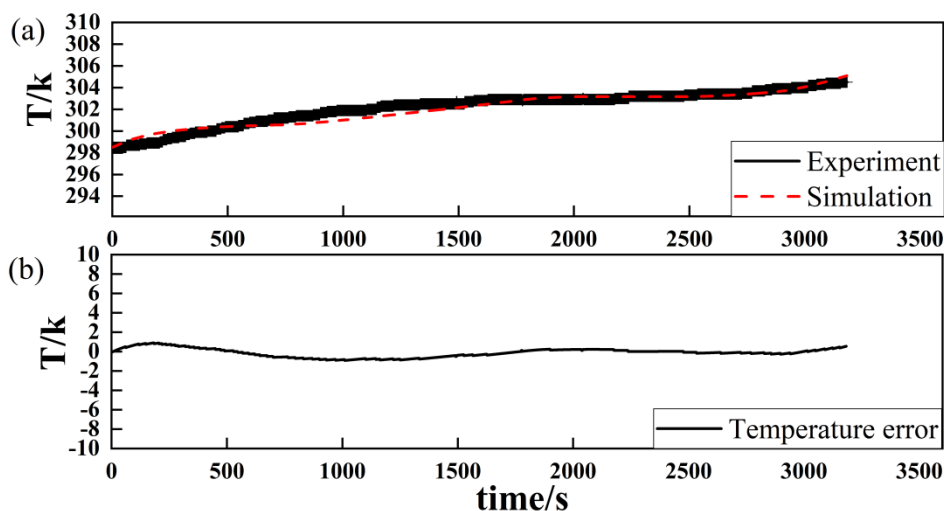


Figure 10. Comparison between the experimental data and simulation results of the test (a) and the absolute temperature error between them (b) at a discharge of 1C.

3.1.2 Verification under the NEDC working condition

To verify the accuracy of the model under actual driving conditions, the tests were conducted under NEDC cycling conditions and compared with the actual external characteristics of the battery.

Figure 11 (a) shows the comparison of curves between the measured and the simulation terminal voltage using the model under the NEDC condition. It can be seen that the simulation value of the model can properly track the experimental value. Both curves include 13 cycles of NEDC conditions. The local voltage around 5600 s has been magnified to analyze and compare the two voltage curves more clearly, and from Figure 11 (c), it can be seen that the two curves basically coincide.

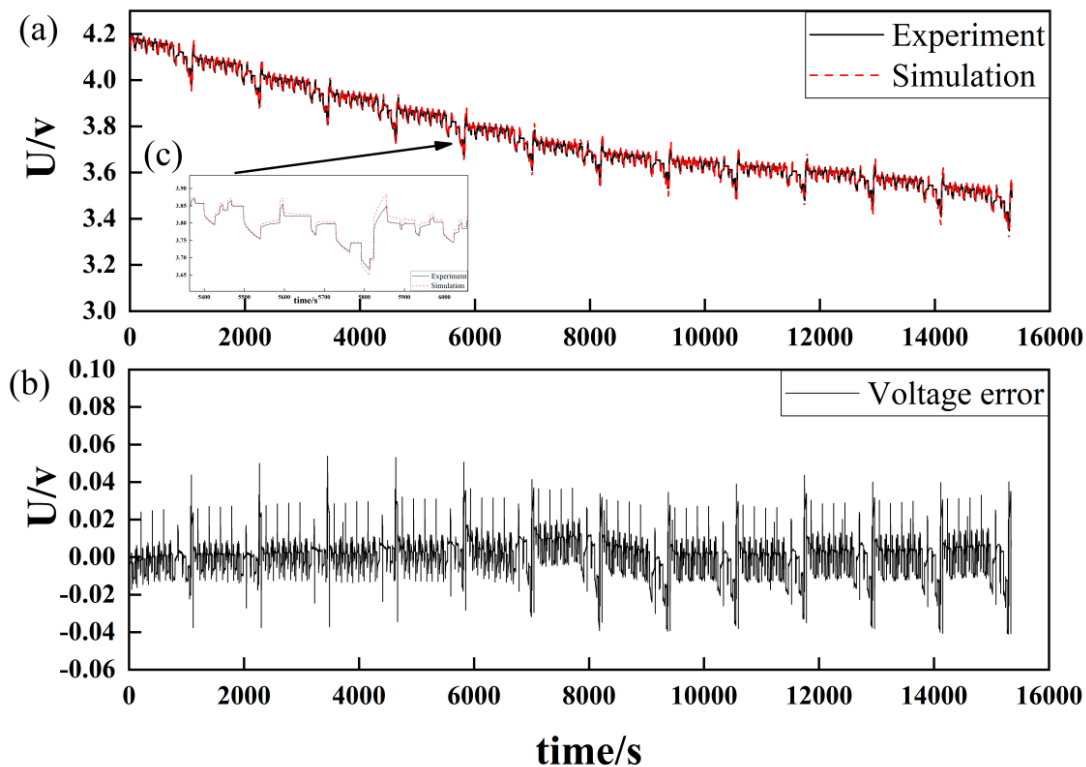


Figure 11. (a) Comparison between the experimental data and simulation results, (b) the voltage error curve of the experiment and simulation, and (c) the local magnification of the curves under the NEDC test condition.

The model voltage error under the NEDC condition is exhibited in Figure 12 (b), and the absolute voltage error of the model is basically kept within 0.02 V; it only reaches 0.06 V in an instant of a high power pulse. Furthermore, the absolute voltage error of the model is kept within 0.04 V with an SOC of 0.3-0.8, which indicates that the established thermoelectric coupling model has good robustness and can accurately simulate the external characteristics of the battery under the NEDC condition.

To evaluate the quality of this model, the simulation results are compared with other related studies, as shown in Table 1. Lithium battery models mainly include two categories: equivalent circuit models [20-23] and electrochemical models [10, 24-28]. Compared with the traditional equivalent circuit model (ECM) [20-23], the influence of temperature changes caused by the battery's own heating is considered in our model, which leads to higher accuracy in simulating the external characteristics of the battery. Electrochemical models include electrochemical models [24-25] and electrochemical thermal coupling models [26-28], depending on whether the battery temperature is considered. The electrochemical thermal coupling model also considers the influence of temperature, which brings a certain improvement in accuracy. However, it is time-consuming and complicated. Our model considers the effect of the battery's own temperature change on the basis of the equivalent circuit, and thus compared with other research reports, it has obvious advantages in simulation accuracy and model simulation time.

Table 1. Comparison with reported works at a discharge of 1C.

References	Model type	Simulation error	Temperature consideration
This paper	Thermoelectric coupling model	0~0.025 V	Yes
10	Electrochemical (Previous work)	0~0.056 V	Yes
20	ECM	0.12% (average)	No
21	ECM with P2D	0~0.06 V	No
22	ECM	0~1.23%/ 0.29% (average)	Yes
23	Composite-ECM	0~2%	No
24	Electrochemical	0~0.08 V	No
25	Electrochemical	0~0.1 V	No
26	Multiphysics-thermal model	0~0.0763 V	Yes
27	Electrothermal	0~1%	Yes
28	Electrochemical-thermal coupling	0~0.07 V	Yes

3.2 Verification of SOC estimation

Accurate SOC estimation is one of the most important functions in a battery management system and is also the basis of many other functions, such as estimating aging life, battery energy management and battery equalization. The establishment of an accurate battery model is the foundation of SOC estimation. In this section, based on the established thermoelectric coupling model, an extended Kalman filter (EKF) algorithm is adopted to estimate the SOC for the nonlinear system of LIBs [29]. This method can effectively restrain the influence of divergence and noise, has good convergence and good applicability.

3.2.1 Definition of battery SOC

The classic definition of SOC is the usable state of charge remaining in the battery, which can be expressed by the following equation:

$$SOC = \frac{Q_{\text{remain}}}{Q_{\text{rated}}} \times 100\% \quad (8)$$

where Q_{rated} is the nominal (rated) capacity of the battery and Q_{remain} is the remaining capacity

in the battery, whose value ranges from 0 to 1; a value of 0 means the battery is empty, and a value of 1 means the battery is fully charged.

3.2.2 SOC Estimation Based on the Extended Kalman Filter

Since the battery itself is a nonlinear system, this paper uses an SOC estimation based on the extended Kalman filter algorithm. The state equations and observation equations of the extended Kalman filter algorithm are as follows:

$$x_k = f(x_{k-1}, u_{k-1}, w_{k-1}) \tag{9}$$

$$z_k = h(x_k, v_k) \tag{10}$$

At each moment, the Taylor equation is used to linearize the equation of state, and the nonlinear system state, shown as equation 9, is transformed into equation 11.

$$x_k = Ax_{k-1} + Bu_{k-1} + w_{k-1} \tag{11}$$

The flow chart of the EKF is shown in Figure 13, and the specific operation steps are as follows:

(1) Initialization:

$$x_0 = E(x_0), P_0 = E[(x_0 - x_0^*)(x_0 - x_0^*)^T] \tag{12}$$

(2) Prediction:

Equation 9 is linearized by a Taylor expansion to obtain an estimate of the state variable at time k:

$$x_k^* = Ax_{k-1} + Bu_{k-1} + w_{k-1} \tag{13}$$

The * sign on the state variable represents that this is the estimated value after the state estimation time is updated; then, the recursive covariance matrix can be obtained:

$$P_k^* = A_k P_{k-1} A_k^T + Q_{k-1} \tag{14}$$

where Q_{k-1} is the covariance of the process excitation noise w_{k-1} of the system: $Q_{k-1} = E(w_{k-1} w_{k-1}^T)$.

(3) The Kalman gain is solved:

$$K_k = P_k^* H_k^T (H_k P_k^* H_k^T + R_k)^{-1} \tag{15}$$

where R_k is the observed noise covariance matrix, $R_k = E(v_k v_k^T)$ and H_k is a Jacobian matrix obtained from the nonlinear relationship of equation 10: $H_k = \left. \frac{\partial h}{\partial x} \right|_{x=x_k^*}$.

(4) Correction:

The state variable and the corresponding covariance matrix are corrected according to the Kalman gain:

$$x_k = x_k^* + K_k (z_k - H_k x_k^*) = x_k^* + K_k (u_k - H_k x_k^*) \tag{16}$$

$$P_k = (I - K_k H_k) P_k^* \tag{17}$$

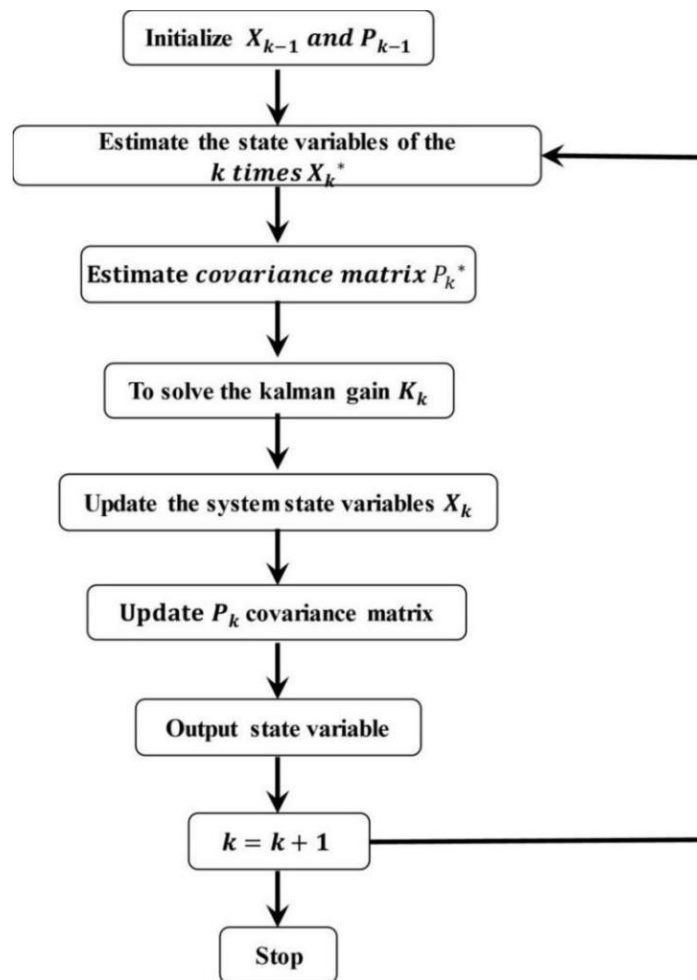


Figure 12. Flow chart of the EKF algorithm.

The SOC estimation of the battery is performed based on the thermoelectric coupling model combined with the EKF algorithm. SOC, U_a and U_b on the two RC networks are taken as the state variables of the system. The working current i of the battery is used instead of U_k as the system excitation because the current is the input of the established thermoelectric coupling model; thus, the above will affect the change of other parameters in the model, including SOC, battery electromotive force and terminal voltage. The observed variable in the algorithm is the terminal voltage U_{oc} , which can be accurately measured by a voltage sensor, while other variables cannot be directly measured externally in the working process of the battery.

3.2.3 Verification of SOC estimation under the NEDC condition

This work verifies the validity of the SOC estimation algorithm of the thermoelectric coupling model under the NEDC condition and compares it with the widely used ampere-time integration that is used in engineering practice. Figure 13 shows the results of the SOC estimation and the corresponding error of batteries obtained by the EKF algorithm and the ampere-hour integration method under the NEDC condition. The SOC reference value is calculated by the classical SOC definition of a battery.

When the initial value is 1, it can be seen that the two curves basically overlap.

Figure 13 (a) is a comparison curve of the EKF estimation results with initial error and no initial error. Figure 13 (c) is a partially enlarged view of four SOC reference curves at the beginning of discharge and the EKF estimation with initial error and no initial error. Although the EKF algorithm estimate curves have little fluctuation around the true value, the overall four curves are substantially coincident. When there is an initial error, the initial SOC changes from 1 to 0.9 or 0.8. Figure 13 (c) shows that the EKF algorithm can quickly converge to the true value and has a good self-correction ability for the initial error value.

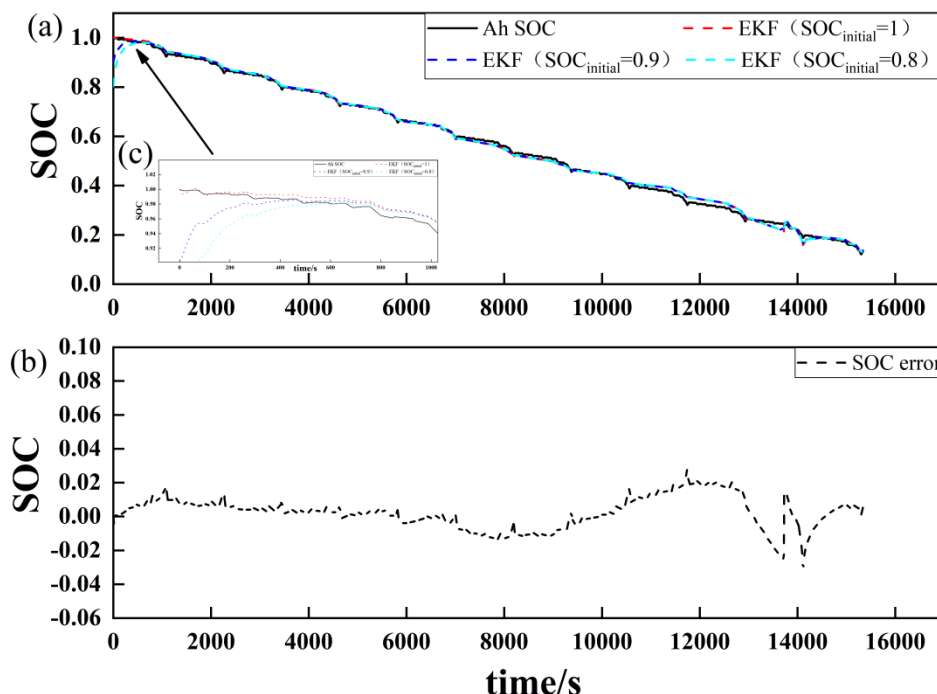


Figure 13. (a) SOC estimation results of EKF, (b) SOC error of EKF with accurate SOC_{initial}, and (c) a local magnification of the SOC estimation result in (a) under NEDC cycling conditions.

Table 2 Comparison of SOC estimation errors between the thermoelectric coupling model and other models.

Model	Intelligent algorithm	Max errors (%)
Thermoelectric coupling model in this paper	EKF	2.96 (NEDC)
Third-order RC circuit model[30]	Sampling point KF	2
Electrical double layer (Previous work)[31]	EKF	2.56 (NEDC)
High accuracy equivalent circuit model (Temperature effect not considered) [32]	EKF	5
Model trained from neural networks[33]	Adaptive EKF	3
Mathematical model[33]	Unscented KF	5

Figure 13 (b) shows the SOC estimation error using the EKF method when there is no initial

error. It can be seen that the method can track the true value well and keep the estimation error within 3%. The average and maximum errors are 0.81% and 2.96%, respectively. The method can effectively estimate the SOC of the battery, is insensitive to initial error, and demonstrates fast convergence. At the same time, the SOC estimation error at the end of discharge becomes large because side reactions in the battery are intensified at a low SOC, and the estimation of the state of the battery is more difficult to obtain. Compared with other models, the thermoelectric coupling model is easy to calculate, while still ensuring accuracy. The outstanding performance of the above model is better than most of the previously reported models (Table 2) [30-33].

4. CONCLUSION

In this study, the influence of temperature increases in the battery itself are considered. A thermoelectric coupling model is established by coupling an equivalent circuit model with a thermal model. The model parameters are identified by a least squares method, and the accuracy of the model is validated by steady-state experiments and dynamic tests. The results indicate that the simulation data are consistent with the experimental results, which can reflect the parameter changes of the battery during the charging and discharging process in real time. Furthermore, the SOC estimation of the battery is carried out under the NEDC condition, which demonstrates that the model has high accuracy, no initial value dependence or cumulative error generated in an ampere-time integration method, has good self-correction ability to the initial value, and can quickly converge to the real value. In addition, the thermal model is based on a mathematical expression with a simple structure and small amount of calculation, which is different from traditional electrochemical heat generation models. Thus, it can be integrated and applied in an actual BMS system and has practical engineering significance.

ACKNOWLEDGMENTS

The research is supported by the NSFC (21501071), the National Science and Technology Foundation of China (2015BAG07B00), the Special Funds for the Transformation of Scientific and Technological Achievements in Jiangsu Province (BA2016162), the Six Talents Peak Project of Jiangsu Province (2016-XNYQC-003, 2015-XNYQC-008), and the Foundation for Advanced Talents of Jiangsu University (13JDG071, 12JDG054).

References

1. L. Lu, X. Han, J. Li, J. Hua and M. Ouyang, *J. Power Sources*, 226 (2013) 272.
2. T. Dagger, P. Miehoff, C. Lurenbaum, F. M. Schappacher and M. Winter, *Energy Technology*, 6 (2018) 2023.
3. V. Ramadesigan, P. W. C. Northrop, S. De, S. Santhanagopalan, R.D. Braatz and V. R. Subramanian, Multi-scale Modeling and Simulation of Lithium-Ion Batteries from Systems Engineering Perspective, 220th ECS Meeting, Boston, America, 2011, Abstract 747.
4. Y. Chen and J. W. Evans, *Electrochimica Acta*, 39 (1994) 517.
5. Y. Chen and J. W. Evans, *J. Electrochem. Soc.*, 141 (1994) 2947.
6. K. J. Lee, K. Smith, A. Pesaran and G. H. Kim, *J. Power Sources*, 241 (2013) 20.
7. M. Doyle and J. Newman, *Electrochimica Acta*, 40 (1995) 2191.
8. T. F. Fuller, M. Doyle and J. Newman, *J. Electrochem. Soc.*, 141 (1994) 1.

9. M. Doyle, T. F. Fuller and J. Newman, *J. Electrochem. Soc.*, 140 (1993) 1526.
10. L. Chen, R. Xu, W. Rao, H. Li, Y.-P. Wang, T. Yang and H.-B. Jiang, *Int. J. Electrochem. Sci.*, 14 (2019) 4124.
11. H. Li, W. Zhang, X. Yang, H. Jiang, Y. Wang, T. Yang, L. Chen and H. Shen, *Electrochimica Acta*, 326 (2019) 134966
12. Y. Chun, B. Wang, H. Zhang, L. Chen and H. Li, *Int. J. Electrochem. Sci.*, 13 (2018) 1131.
13. N. Sato, *J. Power sources*, 99 (2001) 70.
14. S. Yoon, I. Hwang, C. W. Lee, H. S. Ko and K. H. Han, *J. Electroanal. Chem.*, 655 (2011) 32.
15. M. Girtan and M. Rusu, *Sol. Energ. Mat. Sol. C.*, 94 (2010) 446.
16. C. Zhu, X. Li, L. Song and Li. Xiang, *J. Power Sources*, 223 (2013)155.
17. T. I. Evans and R. E. White, *J. Electrochem. Soc.*, 136 (1989) 2145.
18. F. Liu, F. Lan and J. Chen, *J. Mech. Eng.*, 52 (2016) 141.
19. D. Andre, C. Appel and T. Guth, *J. Power Sources*, 224 (2013) 20.
20. X. Zhang, Y. Wang, D. Yang and Z. Chen, *Energy*, 115 (2016) 219.
21. X. Zhang, J. Lu, S. Yuan and X. Zhou, *J. Power Sources*, 345 (2017) 21.
22. Y. Zhang, Y. Shang. N. Cui and C. Zhang, *Energies*, 11 (2018) 19.
23. S. Wang, C. Fernandez, X. Liu, J. Su and Y. Xie, *Meas. Control-Uk*, 51 (2018) 125.
24. Y. Ma, J. Ru, M. Yin, H. Chen and W. Zheng, *J. Appl. Electrochem.*, 46 (2016) 1119.
25. X. Xu, W. Wang and L. Chen, *J. Electrochem. Soc.*, 163 (2016) A1429.
26. L. Zhang, L. Wang, G. Hinds, C. Lyu, J. Zheng and J, Li, *J. Power Sources*, 270 (2014) 367.
27. S. N. Motapon, A. Lupien-Bedard, L. A. Dessaint, H. Fortin-Balanchette and K. Al-Haddad, *IEEE T. Ind. Electron.*, 64 (2017) 998.
28. J. Li, L. Wang, C. Lyu, H. Wang and X. Liu, *J. Power Sources*, 307 (2016) 220.
29. G. L. Plett, *J. Power Sources*, 134 (2004) 262.
30. X. Gao, W. Zhao and Y. Zheng, *Electrochimica Acta*, 295 (2019) 1057.
31. H. He, R. Xiong, X. Zhang, F. Sun and J. Fan, *IEEE Trans. Veh. Technol.*, 60 (2011) 1461.
32. M. Charkhgard and M. Farrokhi, *IEEE Trans. Ind. Electron.*, 57 (2010) 4178.
33. X. Dang, L. Yang and K. Xu, *Electrochimica Acta*, 188 (2016) 356.

© 2020 The Authors. Published by ESG (www.electrochemsci.org). This article is an open access article distributed under the terms and conditions of the Creative Commons Attribution license (<http://creativecommons.org/licenses/by/4.0/>).